

Particle energy cascade in the intergalactic medium

Carmelo Evoli*

Scuola Normale Superiore, Piazza dei Cavalieri 7, 56126 Pisa, Italy

E-mail: evoli@sissa.it

Marco Valdés

Scuola Normale Superiore, Piazza dei Cavalieri 7, 56126 Pisa, Italy

E-mail: marco.valdes@sns.it

Andrea Ferrara

Scuola Normale Superiore, Piazza dei Cavalieri 7, 56126 Pisa, Italy

E-mail: andrea.ferrara@sns.it

We study the development of high energy cascades produced by a primary electron of energy $E_{\text{in}} < 1$ TeV injected into the intergalactic medium (IGM). To this aim we have developed the new code MEDEA (Monte Carlo Energy DEposition Analysis) which includes Bremsstrahlung and Inverse Compton (IC) processes, along with H/He collisional ionizations and excitations, and electron-electron collisions. Our results can be used in many astrophysical contexts, with an obvious application related to the study of decaying/annihilating Dark Matter (DM) candidates in the high- z Universe.

Cosmic Radiation Fields: Sources in the early Universe - CRF2010,

November 9-12, 2010

Desy Germany

*Speaker.

1. Introduction

High energy particles can be produced by several astrophysical and cosmological sources through different acceleration processes. The energy stored in relativistic particles might be a non-negligible fraction of the total energy of these systems and therefore an obvious question arises about how this energy is eventually thermalized and transferred to the surrounding environment. In spite of its importance, this question has received only a relatively limited attention. Previous works have considered non-relativistic initial energies of up to 10 keV, e.g. [8, 2, 11, 4]. In this energy range processes such as free-free emission with charged particles and Inverse Compton (IC) with a diffuse distribution of photons can be safely neglected. However for many astrophysical applications it is necessary to deal with higher energy particles: extrapolating the results and fitting formulae presented in the aforementioned works can lead to substantially incorrect results. It is then important to consider extensions of these works to compute at best the evolution of the energy cascade of relativistic electrons of energy E_{in} into a partially ionized gas under realistic cosmological conditions including the presence of CMB photons.

An astrophysical source of relativistic electrons could come from the decay or annihilation of DM particles. If indeed, as many theoretical models predict, this elusive matter component of the Universe injects relativistic electrons and positrons into the IGM and the consequent inverse Compton scattering with the CMB photons could generate a distortion of the black body spectrum by Sunyaev-Zeldovich (SZ) effect, see e.g. [1, 5].

In the past few years a large number of works has investigated the effects and detectability of DM decays/annihilations into the high redshift IGM via observations of the redshifted 21 cm hyperfine triplet-singlet level transition of the ground state of neutral hydrogen [3, 7, 12, 6]. The interest for such kind of studies is generated by the present or planned construction of large radio interferometers [13]. To understand if observations of the redshifted HI 21 cm line can help constrain DM it is crucial to follow in detail the energy cascade from energetic primary photons or electrons up to energies much higher than previously studied to include those DM candidates that can produce relativistic electrons.

2. Method

Our code MEDEA is based on a Monte Carlo scheme that allows to follow the energy cascade arising from the interaction of relativistic electrons ($E_{\text{in}} < 1$ TeV) with the IGM for $10 < z < 50$. A Monte Carlo method is a computational algorithm that relies on repeated random sampling of the relevant physical quantities and processes (e.g. cross-sections and interaction probabilities) to follow the evolution of the system. Essentially the code calculates for every particle the probability of the main interaction channels and then selects one by a random number generator. Once the reaction happens the code follows the resulting particles to the next interaction, until the energy of the particle drops below a given threshold taken in our case to be 10.2 eV (the Lyman α transition energy), when the photon-gas interaction rate vanishes.

To perform our calculation we implemented in the code a large number of interactions such as collisional ionizations of H, He, HeI; collisional excitations of H, He; electron-electron Coulomb scattering; free-free interactions of electrons with protons; IC with CMB photons; direct collisional

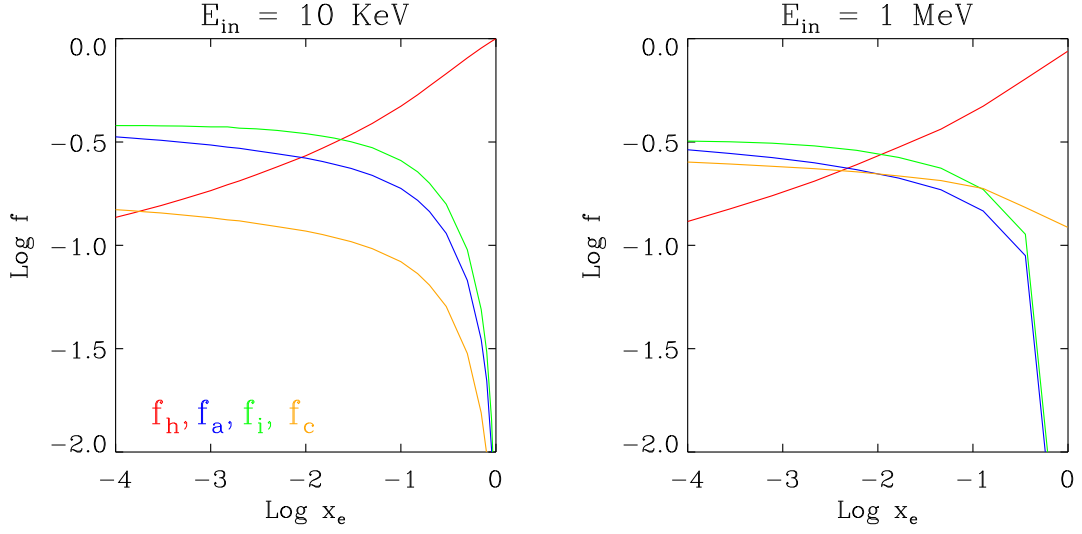


Figure 1: *Left panel:* Fractional energy losses for a primary 10 keV electron. The data points stand for: photons with $E < 10.2\text{eV}$ (orange); gas heating (red); Ly α photons (blue), and ionizations (green). The calculation is performed for 25 values of x_e chosen between $x_e = 0.0001$ and $x_e = 0.99$. *Right:* Same for the case of a 1 MeV primary electron. The fractional energy depositions in this case are calculated for 9 values of x_e chosen between $x_e = 0.0001$ and $x_e = 0.99$.

excitations to the $2s$ level of HI; indirect cascades from $n \geq 3$ states of HI through the $2s$ level; recombinations, see [10] for a detailed description of all these interactions. The energy range of the primary electron is $1 \text{ MeV} < E_{\text{in}} < 1 \text{ TeV}$, the ionized fraction (x_e) considered is $10^{-4} < x_e < 0.99$ and redshift spans $10 < z < 50$. Within these ranges all the other possible interactions of electrons and photons with matter are negligible [14].

3. Results

We present here some of our results for primary electron energies between 1 MeV and 1 TeV and a small number of interesting values of z . The tabulated fractional energy depositions for more different values of z can be downloaded from a dedicated webpage¹. The fraction of the initial electron energy which is deposited into heat, Ly α excitations, ionizations, photons with $E < 10.2 \text{ eV}$, photons with $E > 10^4 \text{ eV}$ and the total energy of CMB photons before they are upscattered will be referred hereafter as f_h , f_a , f_i , f_c , f_{HE} and f_{CMB} respectively.

In Fig. 1 we show the differences between the 10 keV results described in [11], in which the high-energy effects was not taken into account, and the case of $E_{\text{in}} = 1 \text{ MeV}$. The considered redshift is $z = 10$. While f_i , f_a and f_h appear to have similar behaviors in the two cases it is evident that f_c is increased in the 1 MeV plot. The reason for this is the inclusion of IC. The range of energies of the upscattered CMB photons is however very narrow and therefore individual events will enhance the photon energy to values $0.00259\text{eV} \leq h\nu \leq 0.0905 \text{ eV}$. So many CMB photons are upscattered that even though the energy injection from the electrons is small the overall effect

¹<http://wiki.arcetri.astro.it/bin/view/DAVID/MedeaCode>

is still a significant increase of f_c , by a factor ~ 2 for low values of x_e and by over an order of magnitude for $x_e = 0.99$. The reason for the different rise of the curve for low and high values of x_e is simply that IC is not affected by x_e , therefore the curve increases by a fixed value ~ 0.12 with respect to the 10 keV case. When the primary electron energy is degraded by the numerous IC scatterings to values below 10 keV then the secondary cascade behaves consistently with the results shown in the left panel of Fig. 1 and therefore the fractional energy depositions with the exception of f_c retain the same ratios relative to each other. Notice that the process other than IC that produces continuum photons at energies lower than 10.2 eV is, as mention earlier, the two photon forbidden transition $2s \rightarrow 1s$ which we include here and that was neglected in previous studies, e.g. [8].

When a photon is upscattered by IC there are four main energy ranges that we treat differently. Photons with energies below 10.2 eV are added to f_c ; the rare photons with energies between 10.2 eV and 13.6 eV (which we denote as Lyman-continuum photons) are converted into Ly α photons (therefore increasing f_a) while the difference in energy is added to f_c ; photons with $13.6 \text{ eV} \leq h\nu \leq 10^4 \text{ eV}$ are assumed to ionize an atom and are converted into free electrons which we keep following in detail; photons with $h\nu > 10^4 \text{ eV}$ instead free stream into the IGM and are added up to the fraction f_{HE} , see e.g. [14, 9]. Obviously the range of energies will depend on the energy of the primary electron, as the maximum energy of the upscattered photon is proportional to the square of the Lorentz factor or the electron γ_e .

The differences that we identified when going from the 10 keV to the 1 MeV case are sharply enhanced if we consider a higher initial electron energy $E_{\text{in}} = 10 \text{ MeV}$. Inverse Compton remains in fact dominant but the maximum energy that the electron can give to an average $z = 10$ CMB photon is now of the order of 5 eV. This means that there is a dramatic boost in the fractional deposition f_c , which reaches an almost constant value of ~ 0.8 . The other fractional energy curves are left unchanged relative to each other except for f_a which is raised by some CMB photons with higher than average energy that are upscattered to Lyman-continuum values. The 100 MeV case shows curves with very similar properties to the 1 MeV case. The reason for this is that now IC can upscatter photons up to values of a few hundred of eV, which ionize atoms, are converted into electrons and behave as in the left panel of Fig. 1.

Fig. 2 is a summary of our results as it reports the isocontour plot of the fractional energy depositions as a function of both the ionized fraction x_e and the initial electron energy E_{in} . One interesting feature is visible in the panels relative to the fractional energy that goes into ionizations, f_i . At $z = 10$ there is a clear double peak, with the values decreasing sharply for $E_{\text{in}} \sim 10 \text{ MeV}$. This is a behavior that we reported as we commented the second panel in Fig. 1 corresponding to an initial energy of 1 MeV: IC is already dominant but is unable to upscatter CMB photons to energies higher than 10.2 eV. These photons, described by f_c , do not interact further with the IGM and therefore almost 80% of the initial electron energy is lost and the values for the remaining fractional energy depositions decrease sharply. As soon as IC preferentially upscatters photons to energies over 13.6 eV f_i rises again. Notice that at $z = 50$ this double peak effect is not present because CMB photons are more energetic and therefore f_c (second line of panels from the bottom) in the range $1 \text{ MeV} < E_{\text{in}} < 10 \text{ MeV}$ remains higher with respect to the lower z cases. It is also worth noticing that f_c and f_{HE} are essentially independent from x_e but vary slowly with redshift. Intuitively at higher redshift, when CMB photons have higher energies, the value of f_{HE} grows faster with increasing E_{in} .

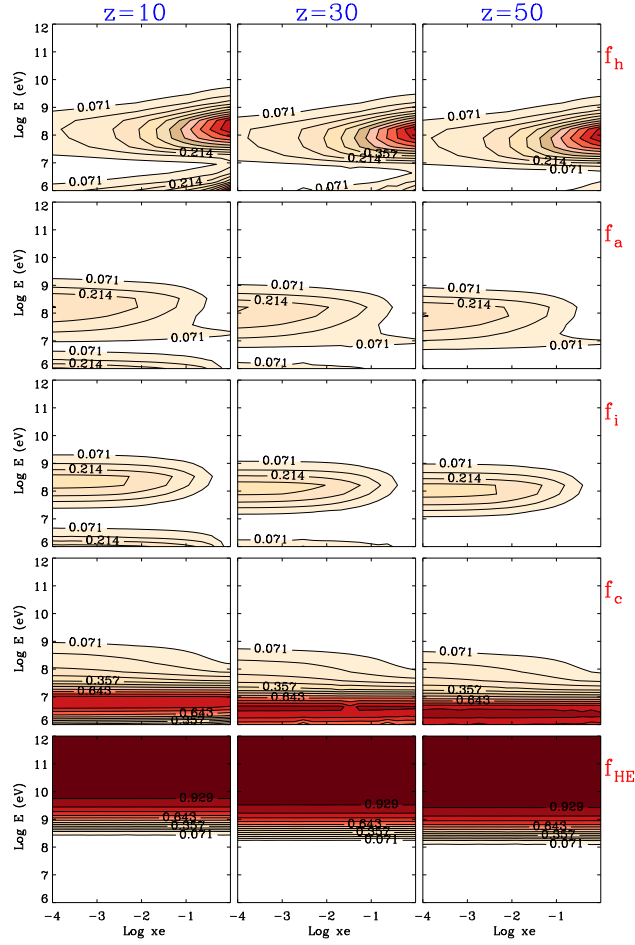


Figure 2: Isocontour plots of the fractional energy depositions as a function of E_{in} and x_e . The panels from top to bottom are relative to f_h , f_a , f_i , f_c , f_{HE} : these are the fraction of the initial electron energy that is deposited into heat, Ly α excitations, ionizations, photons with $E < 10.2$ eV, photons with $E > 10^4$ eV respectively.

4. Conclusions

We have introduced our code MEDEA, based on a Monte Carlo scheme that makes possible to follow the fate of electrons of energies up to 1 TeV in their secondary energy cascade. Our results represent a substantial generalization of previous works that considered exclusively non-relativistic electrons. The results presented here can be used for many astrophysical applications such as cluster radio relics, Active Galactic Nuclei, Stellar flares, Gamma Ray Bursts, Pulsar Wind Nebulae, Supernova Remnants and, more generally, whenever it is necessary to deal with the interaction of energetic and/or relativistic particles with the surrounding thermal gas. A natural application of these results is to study the effects of DM decays/annihilation in the high-redshift universe which we are aiming to investigate in a forthcoming paper.

References

- [1] S. Colafrancesco, S. Profumo, and P. Ullio, *Multi-frequency analysis of neutralino dark matter annihilations in the Coma cluster*, *A&A***455** (2006), 21–43.
- [2] A. Dalgarno, M. Yan, and W. Liu, *Electron Energy Deposition in a Gas Mixture of Atomic and Molecular Hydrogen and Helium*, *ApJS***125** (1999), 237–256.
- [3] S. R. Furlanetto, S. P. Oh, and E. Pierpaoli, *Effects of dark matter decay and annihilation on the high-redshift 21cm background*, *Phys. Rev. D***74** (2006), no. 10, 103502–+.
- [4] S. R. Furlanetto and S. J. Stoeber, *Secondary ionization and heating by fast electrons*, *MNRAS***404** (2010), 1869–1878.
- [5] J. Lavalle, C. Boehm, and J. Barthès, *On the Sunyaev-Zel’dovich effect from dark matter annihilation or decay in galaxy clusters*, *JCAP***2** (2010), 5–+.
- [6] A. Natarajan and D. J. Schwarz, *Dark matter annihilation and its effect on CMB and hydrogen 21cm observations*, *Phys. Rev. D***80** (2009), no. 4, 043529–+.
- [7] Y. A. Shchekinov and E. O. Vasiliev, *Particle decay in the early Universe: predictions for 21 cm*, *MNRAS***379** (2007), 1003–1010.
- [8] J. M. Shull and M. E. van Steenberg, *X-ray secondary heating and ionization in quasar emission-line clouds*, *ApJ***298** (1985), 268–274.
- [9] T. R. Slatyer, N. Padmanabhan, and D. P. Finkbeiner, *CMB constraints on WIMP annihilation: Energy absorption during the recombination epoch*, *Phys. Rev. D***80** (2009), no. 4, 043526–+.
- [10] M. Valdés, C. Evoli, and A. Ferrara, *Particle energy cascade in the intergalactic medium*, *MNRAS***404** (2010), 1569–1582.
- [11] M. Valdés and A. Ferrara, *The energy cascade from warm dark matter decays*, *MNRAS***387** (2008), L8–L12.
- [12] M. Valdés, A. Ferrara, M. Mapelli, and E. Ripamonti, *Constraining dark matter through 21-cm observations*, *MNRAS***377** (2007), 245–252.
- [13] J. S. B. Wyithe, A. Loeb, and D. G. Barnes, *Prospects for Redshifted 21 cm Observations of Quasar H II Regions*, *ApJ***634** (2005), 715–727.
- [14] A. A. Zdziarski and R. Svensson, *Absorption of X-rays and gamma rays at cosmological distances*, *ApJ***344** (1989), 551–566.